OPEN ACCESS

Fresnel's laws in discrete optical media

New Journal of Physics
The open-access journal for physics

Fresnel's laws in discrete optical media

Alexander Szameit[1,5], Henrike Trompeter[1], Matthias Heinrich[1], Felix Dreisow[1], Ulf Peschel[2], Thomas Pertsch[1], Stefan Nolte[1], Falk Lederer[3] and Andreas Tünnermann[1,4]

[1] Institute of Applied Physics, Friedrich-Schiller-Universität Jena, Max-Wien-Platz 1, 07743 Jena, Germany
[2] Institute of Optics, Information and Photonics, Universität Erlangen-Nürnberg, Günther-Scharowsky-Strasse 1/ Bau 24, 91058 Erlangen, Germany
[3] Institute for Condensed Matter Theory and Optics, Friedrich-Schiller-Universität Jena, Max-Wien-Platz 1, 07743 Jena, Germany
E-mail: szameit@iap.uni-jena.de

New Journal of Physics **10** (2008) 103020 (16pp)
Received 25 June 2008
Published 16 October 2008
Online at http://www.njp.org/
doi:10.1088/1367-2630/10/10/103020

Abstract. We present the discrete analog of Snell's refraction law at the interface between two dissimilar waveguide arrays. Additionally, reflection and transmission coefficients for the Bloch waves are derived analytically. The theoretical findings were confirmed by analyzing the evolution of light in femtosecond laser written waveguide arrays.

Contents

[4] Also with: Fraunhofer Institute for Applied Optics and Precision Engineering, Albert-Einstein-Strasse 7, 07745 Jena, Germany.
[5] Author to whom any correspondence should be addressed.

1. Introduction

When light crosses the interface between two dissimilar media, it experiences refraction as well as partial reflection. In dielectric media, these phenomena are described by the famous laws of Snell and Fresnel. When deriving these mathematical expressions, it is implicitly assumed that the media on both sides of the interface are continuous. Hence, assuming a fixed wavelength, they are characterized by a single quantity: the refractive index. However, in modern physics, a variety of more sophisticated systems such as periodically structured media, e.g. photonic crystals (Yablonovitch 1993), constitute an important aspect in many research fields (Busch *et al* 2007). During recent years, a subclass of such periodic media has gained much interest: arrays of evanescently coupled waveguides, which are a representation of so-called discrete systems (Christodoulides *et al* 2003). During recent years, surfaces of and interfaces between waveguide arrays have attracted rapidly growing interest, due to their strong impact on the evolution of light. Light propagation in finite waveguide lattices was modeled in one- (1D) (Makris and Christodoulides 2006) and two-dimensional (2D) (Szameit *et al* 2007) geometries. The tunneling escape from a boundary waveguide was investigated (Longhi 2006) in close analogy to quantum mechanics. Furthermore, the conditions for existence of localized linear modes at defects (Trompeter *et al* 2003) and interfaces (Suntsov *et al* 2007) were analyzed in detail. The research on discrete propagation in waveguide arrays gained further stimulus, when the existence of localized nonlinear modes at surfaces (Kartashov *et al* 2006, Kominis *et al* 2007, Makris *et al* 2005, Molina *et al* 2006, 2007) and interfaces (Makris *et al* 2006, Molina and Kivshar 2007) in waveguide arrays was predicted. These phenomena were experimentally demonstrated in 1D (Iwanow *et al* 2004, Rosberg *et al* 2006, Smirnov *et al* 2006, Suntsov *et al* 2006, 2007) and only recently in 2D (Szameit *et al* 2007, 2008, Wang *et al* 2007). It turned out that light propagation at the interface of two waveguide lattices exhibits a variety of peculiarities as a direct consequence of the discrete nature of the medium. However, to date the transition of light through an interface between two dissimilar waveguide arrays was not analyzed. This is somewhat surprising since one can expect that interfaces also have a strong impact on the refraction, reflection and transmission properties of light, culminating in modifications of the laws of Snell and Fresnel with respect to the continuous case.

In this paper, we bridge this gap and present the discrete version of Snell's law of refraction as well as reflection and transmission coefficients for plane waves passing an interface between two dissimilar waveguide arrays. It will be shown that reflection and refraction are determined by the change of the coupling and the propagation constants at the interface.

2. The discrete Snell's law

In the so-called coupled mode approximation the transverse profile of the propagating modes inside the individual guides is assumed to remain constant, so that only the amplitudes evolve along z. Then one can derive a set of coupled ordinary homogeneous first-order differential equations

$$\mathrm{i}\frac{\mathrm{d}}{\mathrm{d}z}\varphi_m + c(\varphi_{m-1} + \varphi_{m+1}) = 0. \tag{1}$$

Here, φ_m is the amplitude in the mth waveguide and c is the coupling constant, denoting the coupling strength between the individual lattice sites. For reasons of simplicity, the propagation

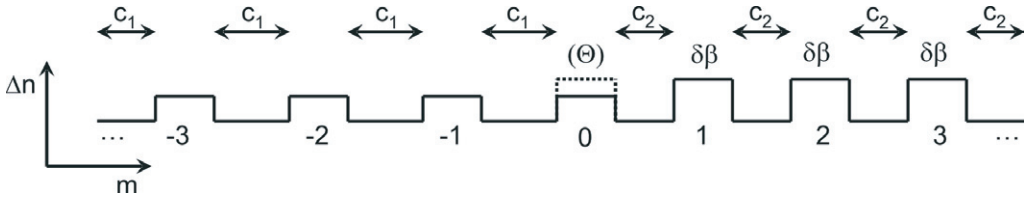

Figure 1. Schematic representation of an interface in a waveguide array, which is induced by a change of the coupling constant and the propagation constants of the guides.

constant β_0 has been removed by a phase transformation. The normalized eigenfunctions of this periodic system are the so-called discrete Bloch waves:

$$\varphi_m = \mathrm{e}^{\mathrm{i}\beta z}\mathrm{e}^{\mathrm{i}\kappa m}. \tag{2}$$

The quantity β is the longitudinal propagation constant and κ denotes the transverse propagation constant multiplied by the waveguide spacing Δ corresponding to a phase difference between adjacent waveguides. Inserting equation (2) into (1), one finds β entirely defined by the dispersion relation

$$\beta = 2c\cos\kappa \tag{3}$$

describing a band structure due to the system's periodicity. All Bloch waves have to fulfill equation (3), otherwise they cannot propagate and decay exponentially.

However, equation (1) describes an infinite system with identical and equally spaced waveguides. Hence, in the presence of an interface, one has to modify these equations. Assuming an interface as depicted in figure 1, the coupled mode equations take the form

$$\begin{aligned}
&(m<0): \ \mathrm{i}\frac{\mathrm{d}}{\mathrm{d}z}\varphi_m + c_1(\varphi_{m-1}+\varphi_{m+1}) = 0,\\
&(m=0): \ \left(\mathrm{i}\frac{\mathrm{d}}{\mathrm{d}z}+\Theta\right)\varphi_0 + c_1\varphi_{-1} + c_2\varphi_1 = 0,\\
&(m>0): \ \left(\mathrm{i}\frac{\mathrm{d}}{\mathrm{d}z}+\delta\beta\right)\varphi_m + c_2(\varphi_{m-1}+\varphi_{m+1}) = 0,
\end{aligned} \tag{4}$$

where $m=0$ is the position of the interface. The quantities c_1 and c_2 are the coupling constants on the two sides of the interface, whereas $\delta\beta$ is the difference of the propagation constants in the isolated waveguides between these two parts of the array (figure 1). If the guide $m=0$ exhibits a detuning $\delta\beta$, the relation $\Theta=\delta\beta$ holds, otherwise $\Theta=0$.

For $\Theta=0$, one obtains two different dispersion relations for both regions with $n<0$ and $n>0$, respectively, which read

$$(m<0): \ \beta_1 = 2c_1\cos\kappa_1, \tag{5}$$

$$(m>0): \ \beta_2 = \delta\beta + 2c_2\cos\kappa_2. \tag{6}$$

Due to translational invariance in the z-direction, the propagation constant β must be conserved in the whole array. Hence, the relation $\beta_1=\beta_2=\beta$ holds, yielding the expression

$$\frac{\cos\kappa_2}{\cos\kappa_1} = \frac{c_1}{c_2} - \frac{\delta\beta}{2c_2\cos\kappa_1}. \tag{7}$$

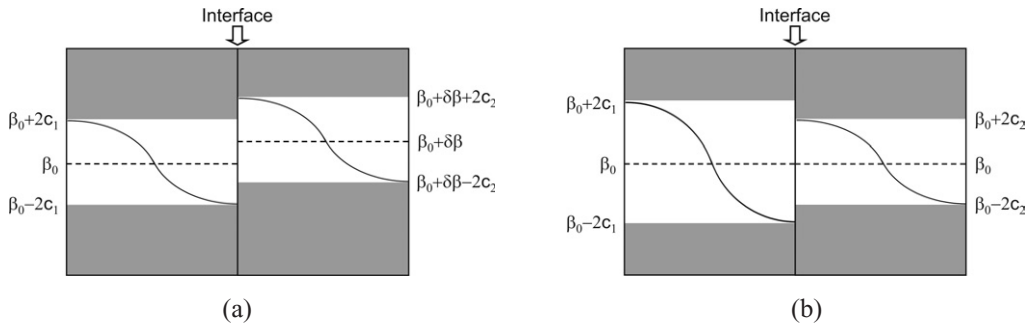

Figure 2. Bandstructure on both sides of the interface. In (a) the band of both sides exhibits the same width ($c_1 = c_2$) but are shifted ($\delta\beta > 0$). In (b) the bands are different in width ($c_1 > c_2$), but are not shifted ($\delta\beta = 0$).

This is the discrete equivalent of the well-known Snell's law, which describes the refraction of a propagating plane wave at an interface between two discrete media. Following this analogy, in the discrete case in equation (7) one has two parameters describing the refraction: the ratio of the coupling constants c_1/c_2 as well as the ratio $\delta\beta/c_2$, which is determined by an additional difference of the waveguide profiles. This is in strong contrast to continuous media, where only the ratio of the refractive indices of both materials affects the refraction at the interface. The actual angle $\alpha_{1,2}$ of the propagation direction of the individual Bloch waves in the respective array region can be easily calculated by (Eisenberg *et al* 2000, Pertsch *et al* 2002, Szameit *et al* 2007)

$$\tan\alpha_{1,2} = \Delta_{1,2}\frac{\partial\beta}{\partial\kappa_{1,2}} = -2\Delta_{1,2}c_{1,2}\sin\kappa_{1,2}. \tag{8}$$

Furthermore, it is evident that only such waves can pass the interface for which $|\cos\kappa_2| \leqslant 1$ holds. Otherwise the Bloch waves experience total internal reflection, since they cannot penetrate the region behind the interface and decay exponentially in this region in the form of evanescent waves. As a peculiar feature of discrete systems it follows from equation (7) that all incoming Bloch waves are reflected totally when

$$|\delta\beta| \geqslant 2(c_1 + c_2). \tag{9}$$

In this particular case, the interface acts as a perfect mirror. Since the coupling constants and the detuning are a function of the wavelength, condition (9) will only be satisfied for a certain range of wavelengths. Hence, this feature may find an application as a spectral filter, where only certain wavelengths can penetrate the interface.

The occurrence of total reflection can be illustrated by means of the band structure. We consider the bands on both sides of the interface according to equations (5) and (6). Since only waves with a positive value of the Bloch vector reach the interface, we examine the bands in the interval $[0; \pi]$. Two examples are shown in figure 2. In figure 2(a) the band is shifted up behind the interface because a positive value for $\delta\beta$ is assumed. In this case, no propagation constant exists inside the right part of the array for Bloch waves from the bottom of the band of the left part. Therefore, such a wave would be completely reflected. An analogous situation occurs for a shrinking of the band due to a decrease of the coupling constant (see figure 2(b)), where total reflection appears if the incoming wave travels at the top or bottom of the respective band.

3. Reflection and transmission coefficients

When the Bloch waves reach the interface, they split into a reflected and transmitted part. The resulting amplitudes of the Bloch waves can be characterized by reflection and transmission coefficients, in close analogy to the Fresnel's formulae at interfaces between continuous media. To calculate these coefficients, for the propagating Bloch waves one uses the ansatz

$$\begin{aligned}(m<0):\ \varphi_m &= \left(\mathrm{e}^{\mathrm{i}\kappa_1 m}+\rho\mathrm{e}^{-\mathrm{i}\kappa_1 m}\right)\mathrm{e}^{\mathrm{i}\beta z},\\ (m=0):\ \varphi_m &= \tau'\mathrm{e}^{\mathrm{i}\beta z},\\ (m>0):\ \varphi_m &= \tau\mathrm{e}^{\mathrm{i}\kappa_2 m}\mathrm{e}^{\mathrm{i}\beta z}.\end{aligned} \tag{10}$$

The coefficient ρ denotes the reflection strength, whereas τ' and τ are the transmission coefficients. Since the guide at $m=0$ can be assumed as a singular defect, one has to consider the transmission into this defect and the $m>0$-region separately. Inserting equations (10) into (4), one obtains

$$a_{-1}:\ -\beta\left(\mathrm{e}^{-\mathrm{i}\kappa_1}+\rho\mathrm{e}^{\mathrm{i}\kappa_1}\right)+c_1\mathrm{e}^{-2\mathrm{i}\kappa_1}+c_1\rho e^{2\mathrm{i}\kappa_1}+c_1\tau'=0, \tag{11}$$

$$a_0:\ (-\beta+\Theta)\,\tau'+c_1\mathrm{e}^{-\mathrm{i}\kappa_1}+c_1\rho\mathrm{e}^{\mathrm{i}\kappa_1}+c_2\tau\mathrm{e}^{\mathrm{i}\kappa_2}=0, \tag{12}$$

$$a_1:\ (-\beta+\delta\beta)\,\tau\mathrm{e}^{\mathrm{i}\kappa_2}+c_2\tau'+c_2\tau\mathrm{e}^{2\mathrm{i}\kappa_2}=0. \tag{13}$$

Equation (11) directly yields

$$\tau'=\frac{\beta}{c_1}\left(\mathrm{e}^{-\mathrm{i}\kappa_1}+\rho\mathrm{e}^{\mathrm{i}\kappa_1}\right)-\mathrm{e}^{-2\mathrm{i}\kappa_1}-\rho\mathrm{e}^{2\mathrm{i}\kappa_1}. \tag{14}$$

When inserting this into equation (12), one obtains

$$\tau=\frac{\mathrm{e}^{-\mathrm{i}\kappa_2}}{c_2}\left[(\beta-\Theta)\left[\frac{\beta}{c_1}\left(\mathrm{e}^{-\mathrm{i}\kappa_1}+\rho\mathrm{e}^{\mathrm{i}\kappa_1}\right)-\mathrm{e}^{-2\mathrm{i}\kappa_1}-\rho\mathrm{e}^{2\mathrm{i}\kappa_1}\right]-c_1\mathrm{e}^{-\mathrm{i}\kappa_1}-c_1\rho\mathrm{e}^{\mathrm{i}\kappa_1}\right]. \tag{15}$$

Using equations (14) and (15), one can resolve equation (13), resulting in

$$\rho=\frac{\left(\left[-\beta+\delta\beta+c_2\mathrm{e}^{\mathrm{i}\kappa_2}\right]/c_2\right)\left((\beta-\Theta)\left[\mathrm{e}^{-\mathrm{i}\kappa_1}-(\beta/c_1)\right]+c_1\right)-(c_2/c_1)\beta+c_2\mathrm{e}^{-\mathrm{i}\kappa_1}}{\left(\left[-\beta+\delta\beta+c_2\mathrm{e}^{\mathrm{i}\kappa_2}\right]/c_2\right)\left((\beta-\Theta)\left[(\beta/c_1)-\mathrm{e}^{\mathrm{i}\kappa_1}\right]-c_1\right)+(c_2/c_1)\beta-c_2\mathrm{e}^{\mathrm{i}\kappa_1}}\mathrm{e}^{-2\mathrm{i}\kappa_1}, \tag{16}$$

where β has to fulfill the dispersion relations (5) and (6). Equations (15) and (16) denote the transmission and reflection coefficients for a Bloch wave crossing an interface as depicted in figure 1 from left to the right. Three examples for the coefficients in dependence of the Bloch vector of the incoming wave are depicted in figure 3.

An interesting issue is the symmetry of the reflection and transmission coefficients around $\kappa_1=\frac{\pi}{2}$, since due to equation (8) this is the maximum angle at which Bloch waves propagate through the array (Pertsch *et al* 2002). In the particular case of a vanishing detuning $\delta\beta=0$, the reflection coefficient simplifies to

$$\rho|_{\delta\beta=0}=\frac{c_1\mathrm{e}^{\mathrm{i}\kappa_1}-c_2\mathrm{e}^{\mathrm{i}\kappa_2}}{c_2\mathrm{e}^{\mathrm{i}\kappa_2}-c_1\mathrm{e}^{-\mathrm{i}\kappa_1}}. \tag{17}$$

This expression, which is the analog of Fresnel's formula for reflection at an interface between two continuous media, is always symmetric around $\kappa_1=\frac{\pi}{2}$, since the reflection is only

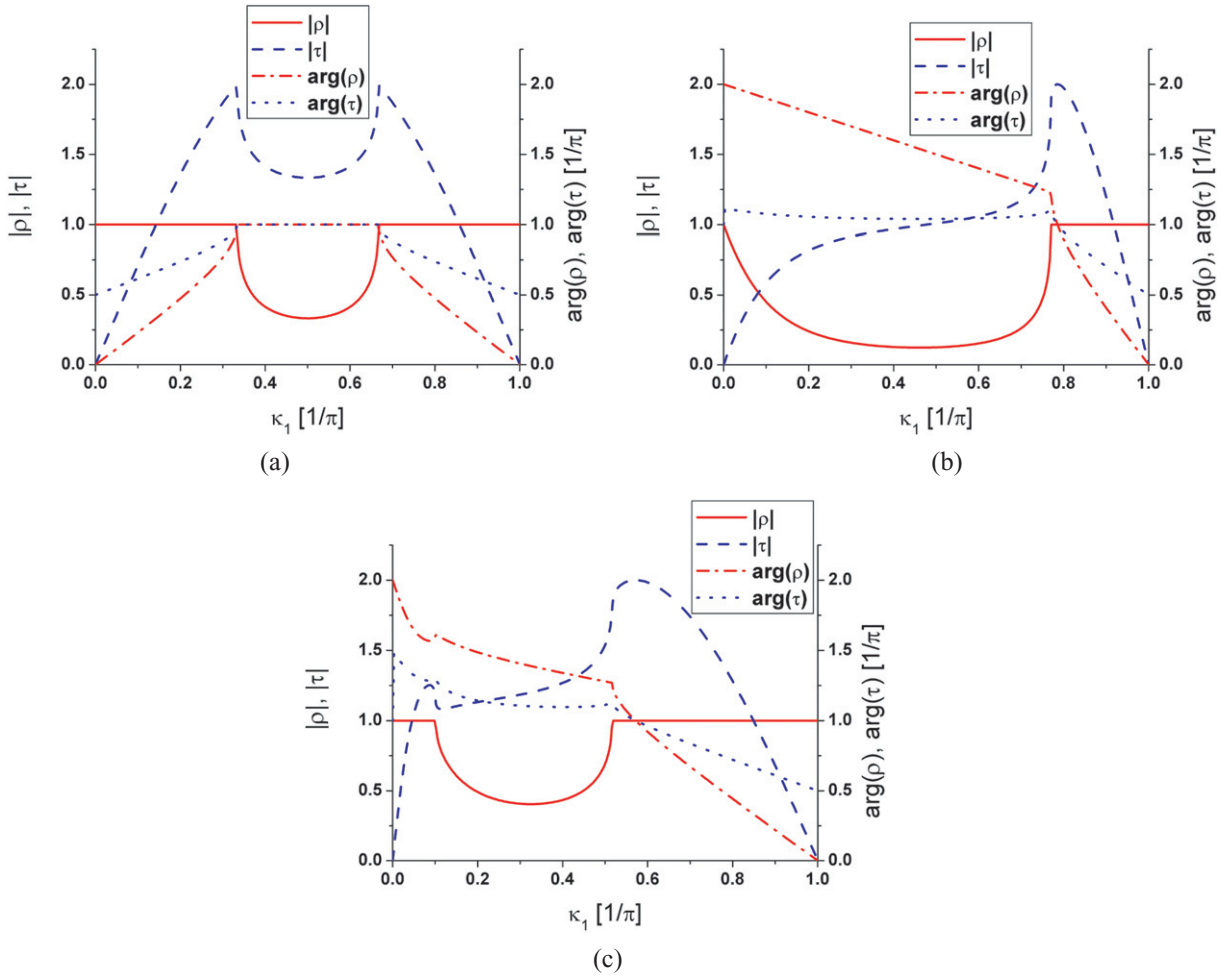

Figure 3. Absolute value (solid) and argument (dashed) of the reflection (red) and transmission (blue) coefficients for (a) $\delta\beta = 0\,\mathrm{cm}^{-1}$, $c_1 = 1\,\mathrm{cm}^{-1}$ and $c_2 = 0.5\,\mathrm{cm}^{-1}$, (b) $\delta\beta = 0.5\,\mathrm{cm}^{-1}$, $c_1 = c_2 = 1\,\mathrm{cm}^{-1}$ and (c) $\delta\beta = 0.9\,\mathrm{cm}^{-1}$, $c_1 = 1\,\mathrm{cm}^{-1}$ and $c_2 = 0.5\,\mathrm{cm}^{-1}$.

dependent on the direction of the incoming wave. Hence, the absolute value $|\rho|$, accounting for the reflected amplitude, as well as the argument $\arg(\rho)$, representing the phase shift due to the reflection, are symmetric, as shown in figure 3(a). This symmetry is broken when $\delta\beta \neq 0$. In this case, it becomes apparent that the phase as well as the amplitude of the reflection (and, hence, also of the transmission) are dependent on the transverse wave vector of the incoming wave rather than on the direction. This is due to the periodic character of waveguide arrays, where different Bloch waves travel in the same direction (see equation (8)).

Concerning the occurrence of total internal reflection, the results are in agreement with the explanation given to figure 2. It might be astonishing that the transmitted wave does not vanish in this case. However, this becomes clear keeping in mind that the transmitted wave has to be either a Bloch wave (for real κ_2) or an evanescent wave decaying exponentially in the case of an imaginary κ_2. As both cases are included, the transmission coefficient τ does not vanish even for total reflection $|\rho| = 1$. To derive a quantity that represents the power conservation, it is useful

to examine the energy flow inside the array. For an infinite array, it follows from equation (1)

$$\begin{aligned} \mathrm{i}\varphi_m^* \frac{\mathrm{d}}{\mathrm{d}z}\varphi_m + c(\varphi_{m-1} + \varphi_{m+1})\varphi_m^* = 0, \\ -\mathrm{i}\varphi_m \frac{\mathrm{d}}{\mathrm{d}z}\varphi_m^* + c(\varphi_{m-1}^* + \varphi_{m+1}^*)\varphi_m = 0. \end{aligned} \tag{18}$$

Subtracting the second from the first equation yields

$$\frac{\mathrm{d}}{\mathrm{d}z}|\varphi_m|^2 = \mathrm{i}c\left[(\varphi_{m-1} + \varphi_{m+1})\varphi_m^* - (\varphi_{m-1}^* + \varphi_{m+1}^*)\varphi_m\right], \tag{19}$$

which denotes the power exchange between a respective guide and its neighbors. The power inside a cluster of guides extending from $-M$ to M is given by

$$Q = \sum_{-M}^{M} |\varphi_m|^2. \tag{20}$$

Power can escape the cluster only via the two outermost waveguides. This is reflected in the corresponding equation

$$\frac{\mathrm{d}}{\mathrm{d}z}Q = \mathrm{i}c\left[(\varphi_{-M}^*\varphi_{-M-1} - \varphi_{-M}\varphi_{-M}^* + \varphi_M^*\varphi_{M+1} - \varphi_M\varphi_{M+1}^*\right], \tag{21}$$

where only the amplitudes of the outermost guides and their neighbors outside the cluster contribute. To determine the power flow one assumes a cluster including all guides from $m = -\infty$ to $m = 0$. The power change of this area, which corresponds to the $(m \leqslant 0)$-region of the array, is given by

$$\left.\frac{\mathrm{d}}{\mathrm{d}z}Q\right|_{m\leqslant 0} = \mathrm{i}c_2\left[\varphi_0^*\varphi_1 - \varphi_0\varphi_1^*\right] = 2c_2\Im\left\{\varphi_0\varphi_1^*\right\}. \tag{22}$$

Assuming plane waves $\varphi_m = \mathrm{e}^{\mathrm{i}\kappa_2 m}$, this equation becomes

$$\left.\frac{\mathrm{d}}{\mathrm{d}z}Q\right|_{m\leqslant 0} = \begin{cases} -2c_2\sin\kappa_2 & (\text{if } \kappa_2 \text{ is real}), \\ 0 & (\text{if } \kappa_2 \text{ is imaginary}). \end{cases} \tag{23}$$

As expected, no power flow exists for evanescent waves (κ_2 imaginary). Assuming that the power transported by the reflected and transmitted wave equals the power of the incoming wave, the coefficients have to fulfill

$$c_1\sin\kappa_1 = |\rho|^2 c_1\sin\kappa_1 + |\tau|^2 c_2\sin\kappa_2. \tag{24}$$

Using equation (7), one finally arrives at

$$1 = |\rho|^2 + \frac{1}{\sin\kappa_1}\sqrt{\left(\frac{c_2}{c_1}\right)^2 - \left(\cos\kappa_1 - \frac{\delta\beta}{2c_1}\right)^2}\,|\tau|^2, \tag{25}$$

which represents the conservation of power inside the array. Hence, the quantities

$$R = |\rho|^2, \tag{26}$$

$$T = \frac{1}{\sin\kappa_1}\sqrt{\left(\frac{c_2}{c_1}\right)^2 - \left(\cos\kappa_1 - \frac{\delta\beta}{2c_1}\right)^2}\,|\tau|^2 \tag{27}$$

represent the reflection and transmission coefficients for the power. As expected, the transmission T grows with decreasing reflection R and vice versa, whereas their sum is constant. The corresponding values for R and T from figure 3 are depicted in figure 4.

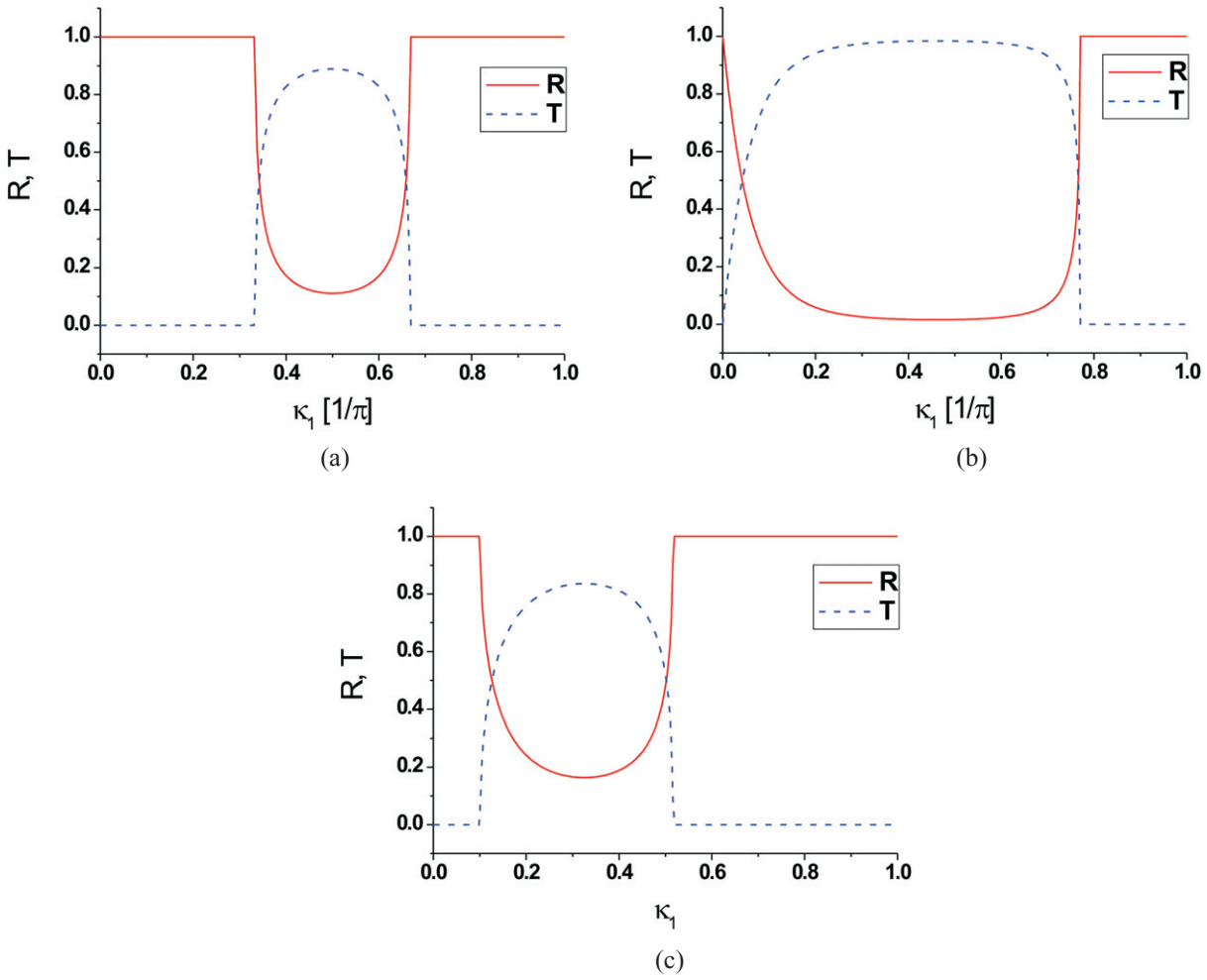

Figure 4. Energy reflection (red) and transmission (blue) coefficients for (a) $\delta\beta = 0\,\mathrm{cm}^{-1}$, $c_1 = 1\,\mathrm{cm}^{-1}$ and $c_2 = 0.5\,\mathrm{cm}^{-1}$, (b) $\delta\beta = 0.5\,\mathrm{cm}^{-1}$, $c_1 = c_2 = 1\,\mathrm{cm}^{-1}$ and (c) $\delta\beta = 0.9\,\mathrm{cm}^{-1}$, $c_1 = 1\,\mathrm{cm}^{-1}$ and $c_2 = 0.5\,\mathrm{cm}^{-1}$.

4. Discussion of the results

To test the analytical results of the previous section, the coupled mode equations (4) were solved numerically. The first point under investigation will be the discrete Snell's law (7). Since this expression is valid for every single Bloch wave, it is useful to analyze this for a broad excitation covering at least five waveguides. In this case, the Fourier spectrum is narrow, so that only a small number of Bloch waves will be excited (Pertsch *et al* 2002). Investigating the evolution of the light inside the array around $\kappa = \pi/2$ diffraction is small due to the significantly reduced curvature of the band in this area (Szameit *et al* 2007). Therefore almost no broadening of the beam appears (see figure 5).

In the array under consideration, on the left side ($m < 0$) the coupling was set to $c_1 = 1\,\mathrm{cm}^{-1}$ for a spacing of $\Delta_1 = 15\,\mu\mathrm{m}$ and on the right side ($m > 0$) to $c_2 = 2\,\mathrm{cm}^{-1}$, according to $\Delta_2 = 11\,\mu\mathrm{m}$ (Szameit *et al* 2007). For these values, in region 1 one obtains a propagation angle of $\alpha_1 = 0.18^\circ$, whereas in the other region $\alpha_2 = 0.25^\circ$, which is shown in

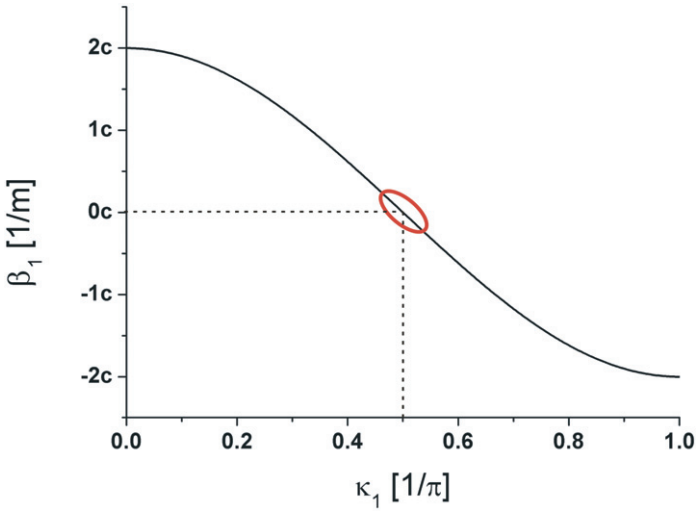

Figure 5. In the vicinity of the normalized transverse wave vector $\kappa = \frac{\pi}{2}$ the second derivative of the longitudinal wave vector vanishes, which is equivalent to diffraction-free propagation.

figure 6(a). The picture changes for an additional detuning of the refractive index in the $m > 0$ region. For a detuning of $\delta n = -1.5 \times 10^{-4}$, the angle of propagation inside this region reduces to $\alpha_2 = 0.23^\circ$ (see figure 6(b)), whereas for an index detuning of $\delta n = -2.7 \times 10^{-4}$, the angle of propagation reduces to $\alpha_2 = 0.18^\circ$, so that no refraction occurs (but still a reflection), which is shown in figure 6(c).

The next peculiar feature of refraction between two discrete media is the fact that the ratio between transmission and reflection is not unique for a specific angle of incidence. In periodic media, the transverse component of the individual Bloch waves range within the first Brillouin zone from $\kappa_{\min} = 0$ to $\kappa_{\max} = \pi$, whereas the angle of propagation (see equation (8)) ranges only from $\alpha_{\min} = 0^\circ$ to $\alpha_{\max} = \arctan\{-2\Delta c\}$, so that two different values of κ yield the same α. Due to equations (16) and (15), in general the reflection and transmission is not symmetric around $\kappa = \frac{\pi}{2}$. Hence, for the same angle α, two different reflection and transmission coefficients exist for two different Bloch waves residing at different positions in the first Brillouin zone. This feature is depicted in figure 7. In an array with $c_1 = 1.05\,\mathrm{cm}^{-1}$, $c_2 = 1.45\,\mathrm{cm}^{-1}$ and a detuning of the refractive index of $\delta n = -2.0 \times 10^{-4}$, two Gaussian excitations with $\kappa_1^{(1)} = \frac{\pi}{3}$ (figure 7(a)) and $\kappa_1^{(2)} = \frac{2\pi}{3}$ (figure 7(b)) propagate at $\alpha = 0.18^\circ$ but exhibit different reflection and transmission coefficients (figure 7(c)).

5. Experimental results

For the experimental verification of these results we used planar waveguide arrays fabricated by the fs laser writing technique (Szameit *et al* 2005, 2006). When ultrashort laser pulses are tightly focused into the bulk material, nonlinear absorption takes place leading to optical breakdown and the formation of a microplasma. Thereby, a permanent change of the material's molecular structure is induced. In the particular case of fused silica, the density is locally increased yielding a positive modulation of the refractive index (Itoh *et al* 2006). By moving the sample transversely with respect to the beam a continuous modification is obtained and a waveguide is

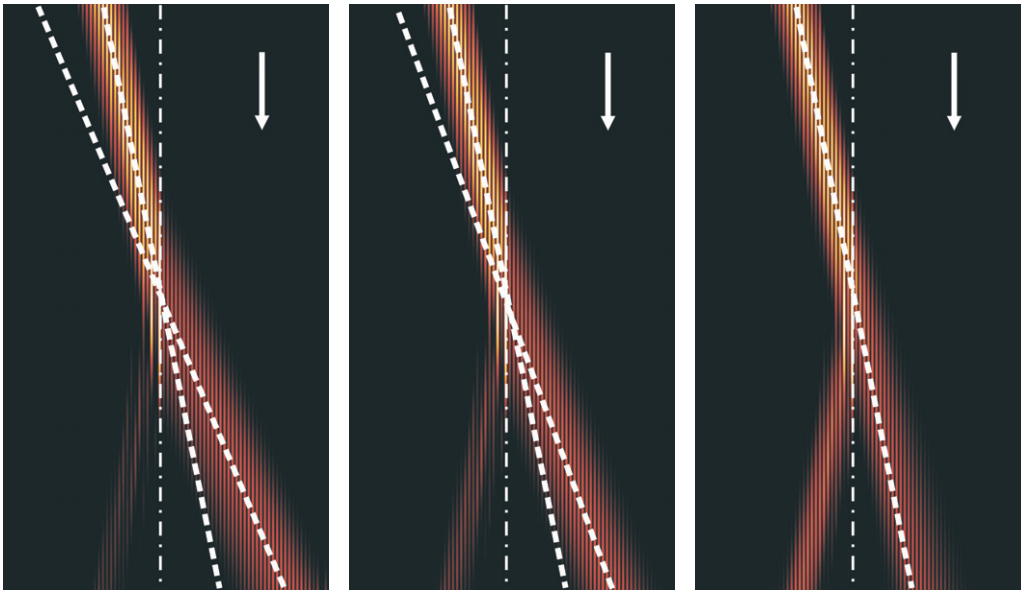

Figure 6. Refraction of a broad Gaussian excitation at an interface between $c_1 = 1\,\mathrm{cm}^{-1}$ and $c_2 = 2\,\mathrm{cm}^{-1}$. In (a) no additional detuning is assumed, in (b) the detuning of the refractive index in the ($m > 0$) region is $\delta n = -1.5 \times 10^{-4}$, whereas in (c) the detuning is $\delta n = 2.7 \times 10^{-4}$. The refraction decreases from (a), where $\alpha_2 = 0.25^\circ$, over (b) with $\alpha_2 = 0.23^\circ$ to (c), where $\alpha_2 = 0.18^\circ$. The propagation direction is marked by the white arrow, whereas the interface is depicted by the dashed-dotted line.

created (Miura *et al* 1997) (see figure 8(a)). By this method, waveguides can be written along arbitrary paths since the only limiting factor in the placement of the focus is the focal length of the writing objective (Nolte *et al* 2003). Since the induced change of the refractive index is a function of the writing velocity (Blomer *et al* 2006), the fs writing technique is in particular well suited to induce defects and interfaces in waveguide arrays. Furthermore, all structural changes are permanent and stable after fabrication (Nolte *et al* 2002). For the fabrication of our waveguides we used a Ti:sapphire laser system (RegA/Mira, Coherent Inc.) with a repetition rate of 100 kHz, a pulse duration of about 150 fs and 0.3 μJ pulse energy at a laser wavelength of 800 nm. The beam was focused into polished fused-silica samples by a 20× microscope objective with a numerical aperture of 0.35. The average power of the laser beam was 32 mW, while the writing velocity was 1300 $\mu\mathrm{m\,s}^{-1}$ resulting in a refractive index change of 6×10^{-4}. The length of all samples was 70 mm. To directly monitor the light propagation we applied a recently developed method of detecting fluorescent light (Szameit *et al* 2007). For that purpose, we used a particular type of fused silica glass with a high content of OH which leads to a massive formation of non-bridging oxygen hole (NBOH) color centers in the modified volume. These can be excited with a HeNe source at 633 nm, which was launched by fiber butt coupling, so that the fluorescence with its maximum at 650 nm can be detected by a camera from above the sample (Dreisow *et al* 2008) (see figure 8(b)).

Two different setups were investigated experimentally (figure 9(a)), with a spacing of 13 μm and 15 μm on the left and right side, respectively. Additionally, in a second sample

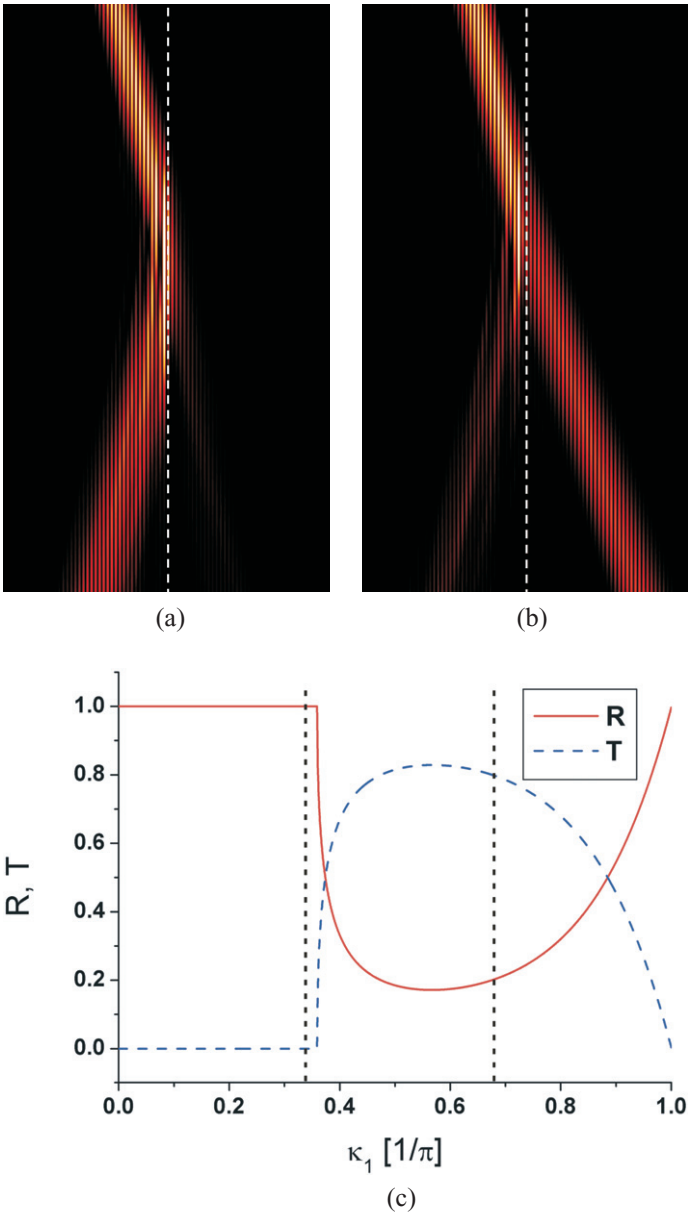

Figure 7. Partial reflection of a broad Gaussian excitation at an interface between two waveguide arrays with $c_1 = 1.05\,\mathrm{cm}^{-1}$, $c_2 = 1.45\,\mathrm{cm}^{-1}$ and a refractive index detuning of -2.0×10^{-4}. In (a) the excitation is centered around $\kappa_1 = \frac{\pi}{3}$ and in (b) around $\kappa_1 = \frac{2\pi}{3}$, yielding in both cases $\alpha = 0.18°$, but different reflection and transmission coefficients, which are depicted in (c). The propagation direction is from top to bottom.

a detuning of the refractive index of $\delta n \approx -2 \times 10^{-4}$ was applied in the region with 13 μm spacing, which was achieved by a slightly higher writing speed of 1800 $\mu\mathrm{m\,s}^{-1}$. The resulting coupling coefficient in the region with $\Delta = 15\,\mu$m is $c_1 = 1.09\,\mathrm{cm}^{-1}$, in the region with $\Delta = 13\,\mu$m is $c_2 = 1.56\,\mathrm{cm}^{-1}$ (Szameit *et al* 2007). These values remain valid even in the case of a slightly negative detuning, since the lower refractive index of the waveguides is compensated

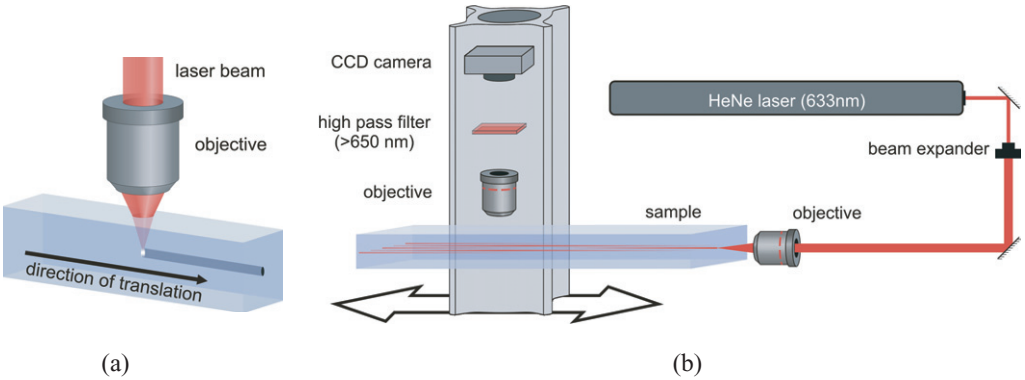

(a) (b)

Figure 8. The principal setup for the fs writing procedure is shown in (a), where the laser beam is focused directly into the glass by a microscope objective. The setup for the fluorescence measurement is sketched in (b). HeNe laser light is launched into the array, while the fluorescent light is monitored by a CCD camera.

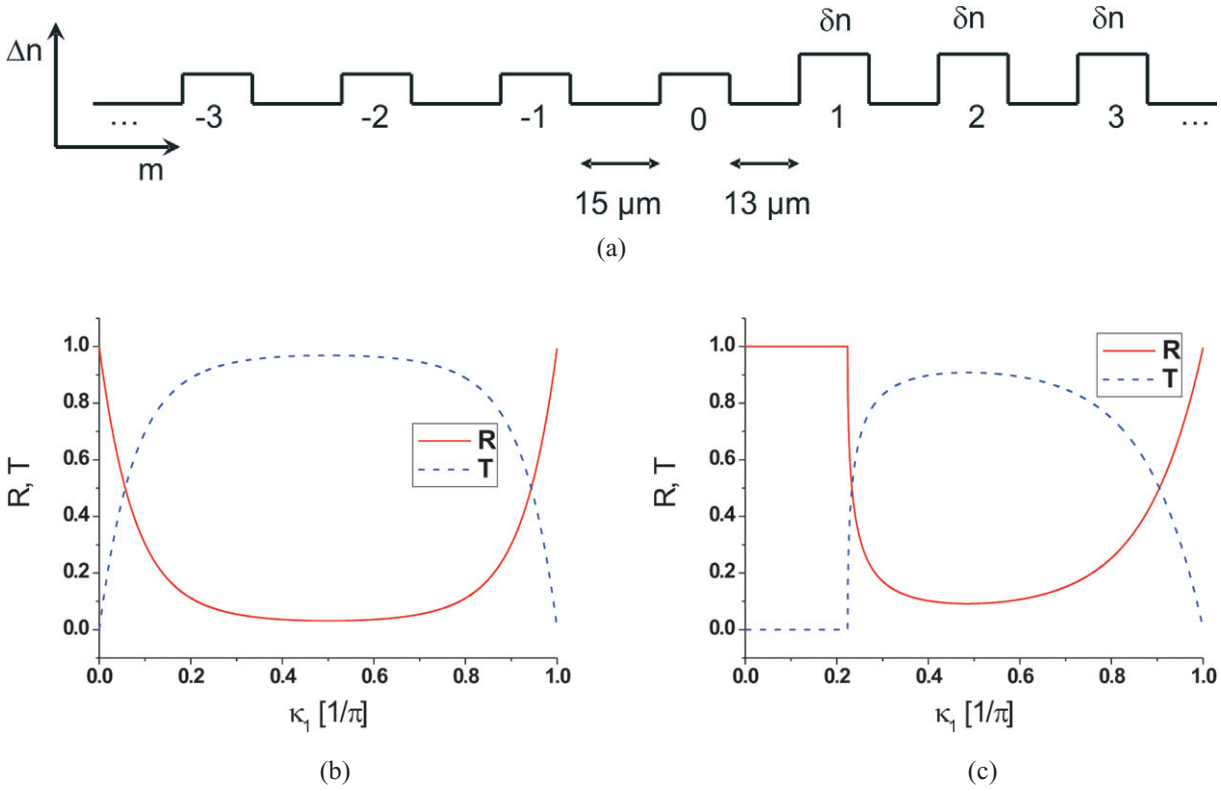

(a) (b) (c)

Figure 9. (a) Schematic representation of the experimentally analyzed waveguide array. On one side the spacing between the waveguides is $\Delta = 15\,\mu$m, whereas on the other side the spacing is $\Delta = 13\,\mu$m. On the latter side, in a second sample, also a small detuning of the refractive index of $\delta n \approx -1.5 \times 10^{-4}$ was applied. The corresponding calculated reflection and transmission coefficients are shown in (b) for $\delta n = 0$ and in (c) for $\delta n \approx -1.5 \times 10^{-4}$.

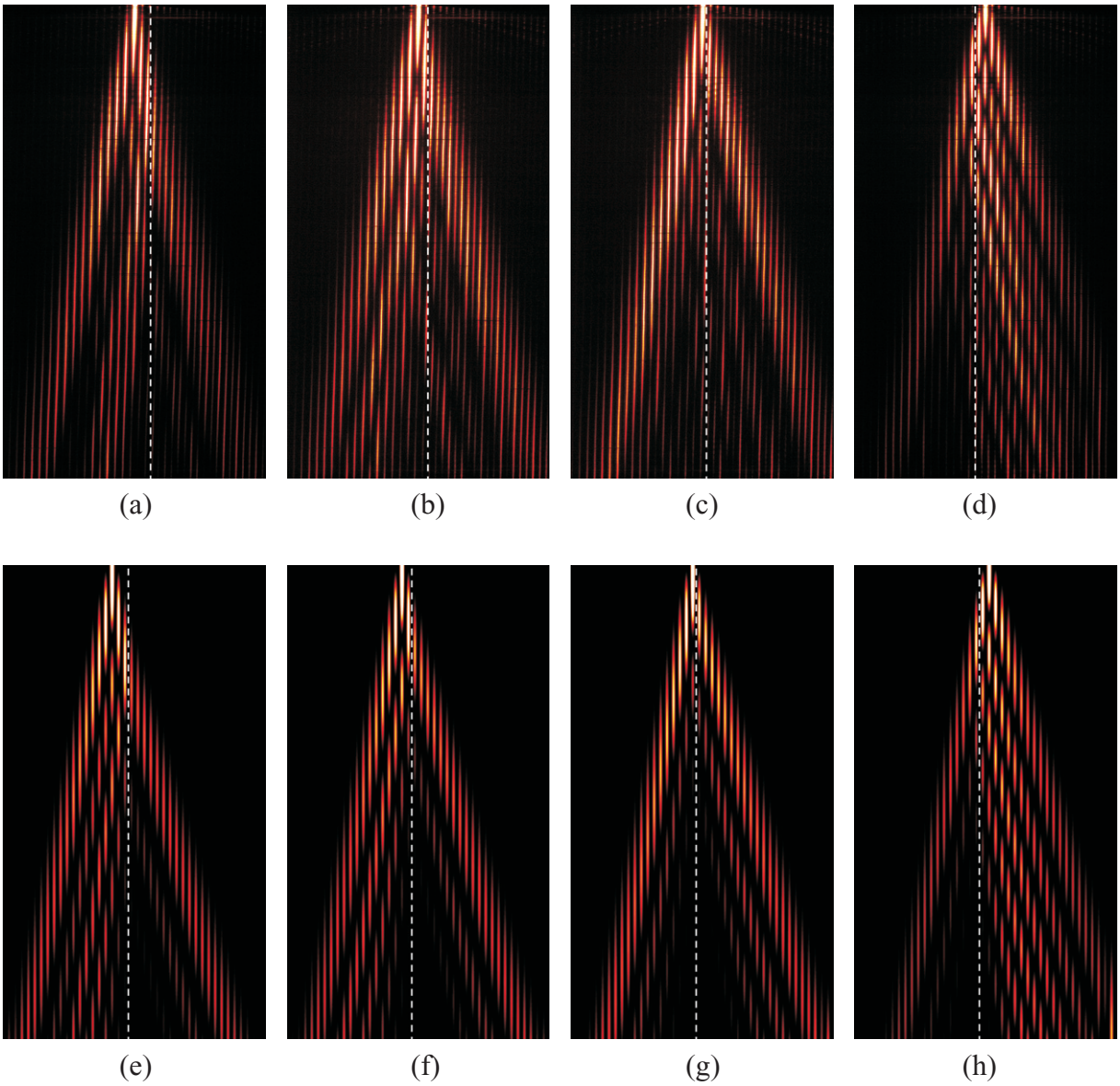

Figure 10. (a)–(d) Experimental fluorescent images of the light propagation in a waveguide array, where $c_1 = 1.09\,\mathrm{cm}^{-1}$ and $c_2 = 1.557\,\mathrm{cm}^{-1}$. The excited waveguide is $m = -3$ (a), $m = -2$ (b), $m = -1$ (c) and $m = 1$ (d). In (e)–(h) the corresponding simulations using equation (4) are shown. The propagation direction is from top to bottom.

by a stronger overlap of adjacent modes. The respective calculated reflection and transmission coefficients of these setups are depicted in figures 9(b) and (c).

The impact of an interface on the propagation of light from a point source (exciting all Bloch waves) without additional detuning ($\delta n = 0$) is demonstrated in figure 10. The experiments illustrate the light evolution for the excitation of waveguide $m = -3$, $m = -2$, $m = -1$ and $m = 1$, shown in figures 10(a)–(d). The corresponding simulations using equation (4) are depicted in figures 10(e)–(h). Depending on the excited waveguide, the light is partially

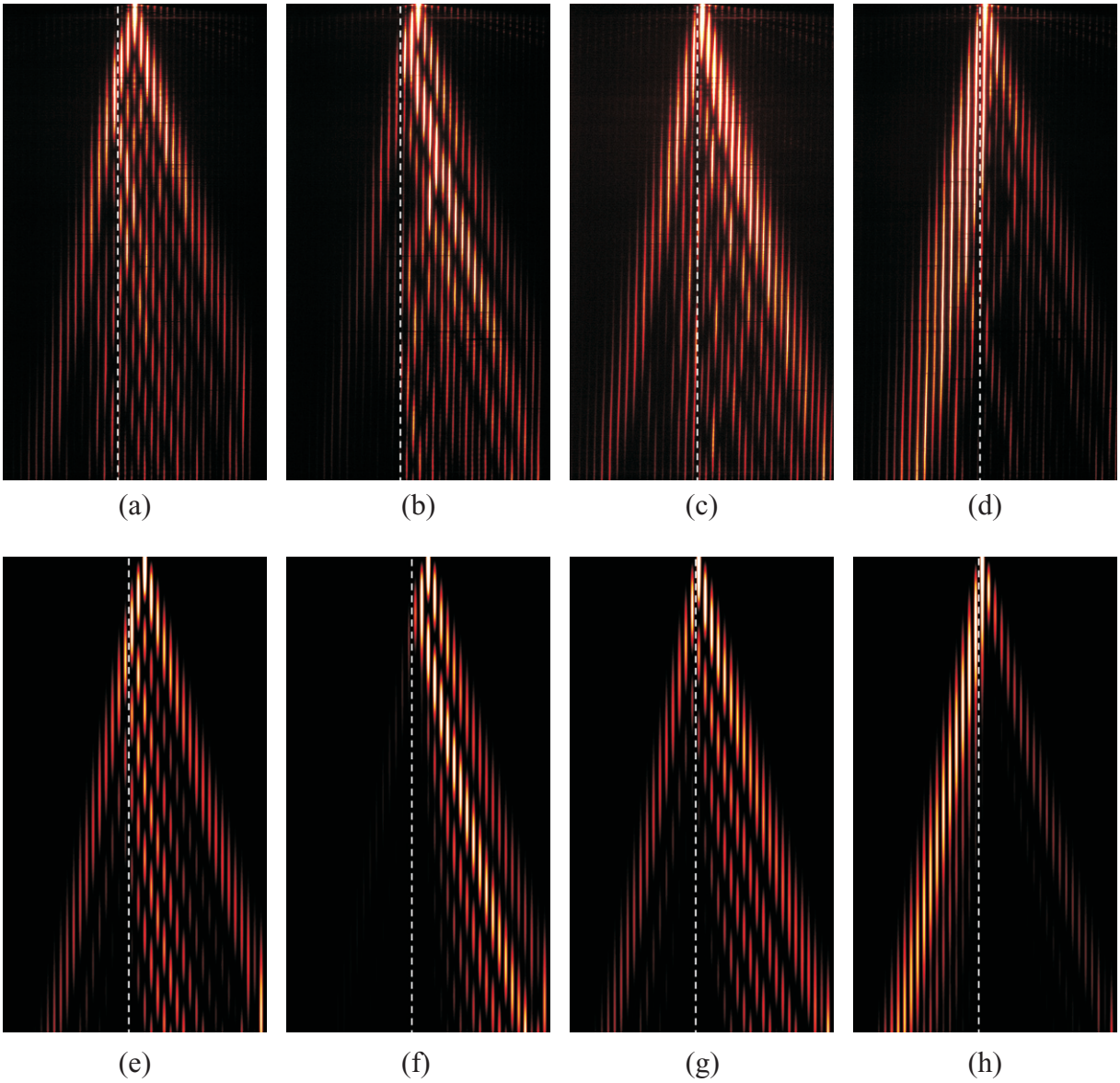

Figure 11. (a)–(d) Experimental fluorescent images of the light propagation in a waveguide array, where $c_1 = 1.09\,\mathrm{cm}^{-1}$ and $c_2 = 1.557\,\mathrm{cm}^{-1}$. In (a) and (b) the excited waveguide is $m = 2$, whereas in (c) and (d) this is $m = 0$. Furthermore, in (b) and (d) an additional detuning of $\delta n \approx -2 \times 10^{-4}$ is applied. The corresponding simulations are shown in (e)–(h). The propagation direction is from top to bottom.

reflected at the interface. From figure 9(b) it follows that in particular the side lobes at $\kappa = \frac{\pi}{2}$ are almost entirely transmitted and only slightly refracted from $\alpha_1 = 0.18^\circ$ to $\alpha_1 = 0.23^\circ$. In contrast, the Bloch waves in the center and the edge of the Brillouin zone experience strong reflection. This is supported by the observation that a large fraction of the light between the side lobes, which results from these Bloch waves, remains in this semi-array where the excited waveguide is located.

This picture changes when an additional detuning $\delta n \approx -2 \times 10^{-4}$ is introduced in the $(m > 0)$-region, since in this case the reflection and transmission coefficients are modified (figure 9(c)). The experimentally observed light evolution from a point source in such an array is depicted in figure 11(b) for the excited waveguide at $m = 2$ and figure 11(d) with the light launched in waveguide $m = 0$. The corresponding simulations are shown in figures 11(f) and (h). The experimental propagation pattern of the undetuned array is presented in figures 11(a) and (c) for the excited waveguide at $m = 2$ and $m = 0$, respectively. The corresponding simulations are given in figures 11(e) and (g). The main feature is now that in the detuned array the reflection is much stronger for all Bloch waves, so that almost all of the incident light is reflected at the interface (figures 11(b) and (d)). Additionally, due to equation (7), the angle of propagation in the detuned array region changes to $\alpha_1 = 0.20°$. This points out again that in discrete media there are two quantities which characterize the light evolution: the coupling strength and an additional detuning of the propagation constant.

6. Conclusions

We have presented the discrete analog of Snell's refraction law at an interface. It was shown that the refraction is characterized by two quantities: the coupling strength and an additional detuning of the propagation constant, in contrast to continuous media. Additionally, refraction and transmission coefficients for the Bloch waves and the power were introduced as the discrete analog of Fresnel's formulae. The results were experimentally verified in fs laser written waveguide arrays, where the light propagation was directly monitored using fluorescent light.

Acknowledgment

We acknowledge support by the Deutsche Forschungsgemeinschaft (Research Group 'Nonlinear spatial-temporal dynamics in dissipative and discrete optical systems' FG 532).

References

Blomer D, Szameit A, Dreisow F, Schreiber T, Nolte S and Tuennermann A 2006 *Opt. Express* **14** 2151–7
Busch K, von Freymann G, Linden S, Mingaleev S, Tkeshelashvili L and Wegener M 2007 *Phys. Rep.* **444** 101–202
Christodoulides D, Lederer F and Silberberg Y 2003 *Nature* **424** 817–23
Dreisow F, Heinrich M, Szameit A, Doering S, Nolte S, Tuennermann A, Fahr S and Lederer F 2008 *Opt. Express* **16** 3474–83
Eisenberg H, Silberberg Y, Morandotti R and Aitchison J 2000 *Phys. Rev. Lett.* **85** 1863–6
Itoh K, Watanabe W, Nolte S and Schaffer C 2006 *MRS Bull.* **31** 620–5
Iwanow R, Schieck R, Stegeman G, Pertsch T, Lederer F, Min Y and Sohler W 2004 *Phys. Rev. Lett.* **93** 113902
Kartashov Y, Vysloukh V and Torner L 2006 *Phys. Rev. Lett.* **96** 073901
Kominis Y, Papadopoulos A and Hizanidis K 2007 *Opt. Express* **15** 10041–51
Longhi S 2006 *Phys. Rev.* E **74** 026602
Makris K and Christodoulides D 2006 *Phys. Rev.* E **73** 036616
Makris K, Hudock J, Christodoulides D, Stegeman G, Manela O and Segev M 2006 *Opt. Lett.* **31** 2774–6
Makris K, Suntsov S, Christodoulides D and Stegeman G 2005 *Opt. Lett.* **30** 2466–8
Miura K, Qui J, Inoue H, Mitsuyu T and Hirao K 1997 *Appl. Phys. Lett.* **71** 3329–31
Molina M, Kartashov Y, Torner L and Kivshar Y 2007 *Opt. Lett.* **32** 2668–70
Molina M and Kivshar Y 2007 *Phys. Lett.* A **362** 280–2

Molina M, Vicencio R and Kivshar Y 2006 *Opt. Express* **31** 1693–5
Nolte S, Will M, Burghoff J and Tuennermann A 2003 *Appl. Phys.* A **77** 109–11
Nolte S, Will M, Chichkov B and Tuennermann A 2002 *Proc. SPIE* **4637** 188–96
Pertsch T, Zentgraf T, Peschel U, Braeuer A and Lederer F 2002 *Phys. Rev. Lett.* **88** 093901
Rosberg C, Neshev D, Krolikowski W, Mitchell A, Vicencio R, Molina M and Kivshar Y 2006 *Phys. Rev. Lett.* **87** 083901
Smirnov E, Stepic M, Rueter C, Kip D and Shandarov V 2006 *Opt. Lett.* **31** 2338–40
Suntsov S, Makris K, Christodoulides D, Stegeman G, Hache A, Morandotti R, Yang H, Salamo G and Sorel M 2006 *Phys. Rev. Lett.* **96** 063901
Suntsov S, Makris K, Christodoulides D, Stegeman G, Morandotti R, Volatier M, Aimez V, Ares R, Rueter C and Kip D 2007 *Opt. Express* **15** 4663–70
Suntsov S, Makris K, Christodoulides D, Stegeman G, Morandotti R, Yang H, Salomo G and Sorel M 2007 *Opt. Lett.* **32** 3098–110
Szameit A, Bloemer D, Burghoff J, Pertsch T, Nolte S and Tuennermann A 2006 *Appl. Phys.* B **82** 507–12
Szameit A, Bloemer D, Burghoff J, Schreiber T, Pertsch T, Nolte S, Tuennermann A and Lederer F 2005 *Opt. Express* **13** 10552–7
Szameit A, Dreisow F, Hartung H, Nolte S, Tuennermann A and Lederer F 2007 *Appl. Phys. Lett.* **90** 241113
Szameit A, Dreisow F, Pertsch T, Nolte S and Tuennermann A 2007 *Opt. Express* **15** 1579–87
Szameit A, Kartashov Y, Dreisow F, Heinrich M, Vysloukh V, Pertsch T, Nolte S, Tuennermann A, Lederer F and Torner L 2008 *Opt. Lett.* **33** 663–5
Szameit A, Kartashov Y, Dreisow F, Pertsch T, Nolte S, Tuennermann A and Torner L 2007 *Phys. Rev. Lett.* **98** 173903
Szameit A, Pertsch T, Dreisow F, Nolte S, Tuennermann A, Peschel U and Lederer F 2007 *Phys. Rev.* A **75** 053814
Trompeter H, Peschel U, Pertsch T, Lederer F, Streppel U, Michaelis D and Braeuer A 2003 *Opt. Express* **11** 3404–11
Wang X, Bezryadina A, Chena Z, Makris K, Christodoulides D and Stegeman G 2007 *Phys. Rev. Lett.* **98** 123903
Yablonovitch I 1993 *J. Opt. Soc. Am.* B **10** 283–95